International Journal for Innovation Education and Research

ONLINE ISSN: 2411-2933 PRINT - ISSN: 2411-3123

Remote and Safe Monitoring of Magnetic Fields Produced by Transmission Lines in Areas of High Concentration of Lightning Strokes

Carlos Alberto T. Carvalho Jr.;Ciro J. Egoavil;Frank Gonzatti;Felix A. Farret

Abstract

Monitoring of magnetic and electric fields in high voltage transmission lines (HVTL) of power plants and substations (SEs) is contemplated by Brazilian Regulatory Standard 616/2014. The measurement procedures of the magnetic and electric fields in SEs must follow a methodology in case of continuous field monitoring of the power equipment where it is common lightning stroke incidences. These monitoring procedures must be carried out in such a way that the recording of electromagnetic fields is done without necessity of exposuring the technical team to irradiation from the equipment and machines generating electrical power. This paper describes a prototype which is able to produce data at a specified safe distance from the irradiating area. The experimental recorded data was acquired, processed, compared and analyzed in areas of more intense radiation levels, acceptable levels and safe levels. This work aimed to establish basis of a technological innovation for the continuous recording of electromagnetic data, trying to cover the surroundings of transmission lines in urban environments, close to the generating units and substation installations wherever the highest levels of magnetic field could be found.

Keyword: Magnetic field monitoring; overhead transmission lines; lightning stroke areas; monitoring electromagnetic

Published Date: 2/28/2018 **Page.99-115** **Vol 6 No 02 2018**

Link: http://ijier.net/ijier/article/view/953

Remote and Safe Monitoring of Magnetic Fields Produced by Transmission Lines in Areas of High Concentration of Lightning Strokes

Carlos Alberto T. Carvalho Jr., Ciro J. Egoavil
Universidade Federal de Rondônia
Brazil

Frank Gonzatti, Felix A. Farret
Federal University of Santa Maria
Brazil

Abstract

Monitoring of magnetic and electric fields in high voltage transmission lines (HVTL) of power plants and substations (SEs) is contemplated by Brazilian Regulatory Standard 616/2014. The measurement procedures of the magnetic and electric fields in SEs must follow a methodology in case of continuous field monitoring of the power equipment where it is common lightning stroke incidences. These monitoring procedures must be carried out in such a way that the recording of electromagnetic fields is done without necessity of exposuring the technical team to irradiation from the equipment and machines generating electrical power. This paper describes a prototype which is able to produce data at a specified safe distance from the irradiating area. The experimental recorded data was acquired, processed, compared and analyzed in areas of more intense radiation levels, acceptable levels and safe levels. This work aimed to establish basis of a technological innovation for the continuous recording of electromagnetic data, trying to cover the surroundings of transmission lines in urban environments, close to the generating units and substation installations wherever the highest levels of magnetic field could be found.

Keywords: Magnetic field monitoring; overhead transmission lines; lightning stroke areas; monitoring electromagnetic waves.

1. Introduction

People interactions to electromagnetic fields (EMF) in the surroundings of overhead power lines (50 or 60 Hz) is a subject of concern and study since the end of the last century. Epidemiological studies have been inconclusive to associate exposition to extremely low frequency EMF (ELF) generated by exposure to electrical equipment and proximity of high-voltage transmission lines and certain types of cancers for the occupational population [1]. Also, the scientific community's is still concerned about exposurement to ELF magnetic fields manifested in several publications as the possible cause of other diseases such as Alzheimer's [2], biological effects by altering intracellular calcium homeostasis [3], changes in neuronal activity [4], disturbances in sleep quality [5], changes in skeletal development in rodent embryos, general

cancer, heart rate variability, behavioural changes such as suicide and depression, hypersensitivity, humoral cognitive changes such as those compiled by IARC International Agency for Research on Cancer [6].

Aware of the scientific community concerns and applying the Precautionary Principle [7] in an attempt to reduce possible effects of EMF on human beings, WHO has established the reference limits for the general and occupational public of exposition to the EMF-ELF levels drawn up by ICNIRP through some guidelines published in 1998 [8] and 2010 [9]. In the last update, Table 1 emphasizes that the reference levels to magnetic fields has had significant changes along the years.

Table 1. Reference levels adopted by ICNIRP for the magnetic field [8], [9].

ICNIRP GUIDELINES	**Magnetic Field Density (μT)**	
	1998	**2010**
General Public	83.33	200
Occupational Public	416.67	1000

The table information is worrying and after reviewing the survey conducted by the EMF-Portal in 2014, showing that less than 50% of 56 countries met WHO guidelines [10].

Other relevant information that must be considered is the electromagnetic field levels dynamics close to overhead transmission lines depends on many parameters such as: the configuration of the cross sectional of the transmission line; voltage level; load current and the effect of imbalances; conductor types; soil resistivity; and metal structure effects near power transmission lines, such as constructions and pipelines [11]. Therefore, the electromagnetic field generated by TL in the area under analysis should be estimated and simulated at the project stage to assure that the field intensities should not exceed the reference values specified by ICNIRP [9].

This paper presents some results of a prototype to estimate continuous and safe electromagnetic field irradiation in environments close to high alternating voltage and high frequency concentration levels, specifically in the vicinity of overhead power transmission lines.

2. Analytical calculation of magnetic flux density

Khawaja and Huang [12] reviewed the influence of magnetic flux density from catenary suspended between two transmission towers. The effect in point (x_o, y_o, z_o) of Figure 1 can be calculated using Biot-Savart's Law.

$$d\vec{B}_i = \frac{\mu_0 I_i}{4\pi|\vec{r}|^3}\left(d\vec{l}_i \times \vec{r}\right) \quad (1)$$

where $d\vec{l}_i$ can be decomposed in orthogonal coordinates as:

$$d\vec{l}_i = dx_i\hat{\imath}_x + 0\hat{\imath}_y + dz_i\hat{\imath}_z \tag{2}$$

with:

$$d\vec{l}_i = dx_i\hat{\imath}_x + 0\hat{\imath}_y + \frac{dz_i}{dx_i}dx_i\hat{\imath}_z \tag{3}$$

Catenary equation in coordinates system is:

$$z_i = \frac{1}{\alpha}(\cosh(\alpha x_i) - 1), \quad -\frac{L}{2} \le x_i \le \frac{L}{2} \tag{4}$$

where α (conductor linear weight/traction) is a constant determinate by the transmission line mechanical parameters and L is the span between towers. Deriving (4) with respect to *x* we have (6).

$$\frac{dz_i}{dx_i} = \sinh(\alpha x_i) \tag{5}$$

Vector $\vec{r}$ is given by (6).

$$\vec{r} = (x_0 - x_i)\hat{\imath}_x + (y_0 - y_i)\hat{\imath}_y + (z_0 - z_i)\hat{\imath}_z \tag{6}$$

In Figure 1 is shown a simplified representation of a TL to calculate $d\vec{B}_i$ at a particular monitoring point i as generated by one single generic phase conductor**.**

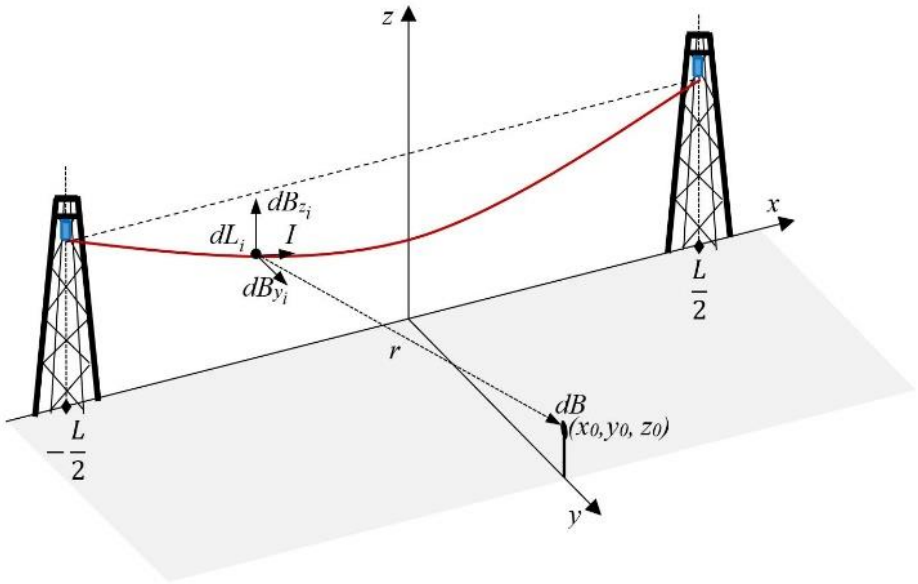

Figure 1 Assessment of the magnetic density B at the monitoring point.

In this analysis it is considered a differential magnetic field ($d\vec{B}_i$) generated by a differential section

of length ($d\vec{l}i$) at a distance ($\vec{r}$), when a current (I) circulates through a phase conductor point (i).

Substituting $d\vec{l}i$ and $\vec{r}$ in $d\vec{B}_i$, the magnetic flux density can be assessed for the conductor phase at (i) of the line transmission by (7). In this relationship are represented these three components in a simplified way.

$$\vec{B}_i = \frac{\mu_0 I_i}{4\pi} \int_{-\frac{L}{2}}^{\frac{L}{2}} \begin{Bmatrix} \frac{[-\sinh(\alpha x_i)\,(y_0 - y_i)]}{|\vec{r}|^3}\hat{\imath}_x + \\ \frac{[(x_0 - x_i)\sinh(\alpha x_i) - (z_0 - z_i)]}{|\vec{r}|^3}\hat{\imath}_y \\ -\frac{(y_0 - y_i)}{|\vec{r}|^3}\hat{\imath}_z \end{Bmatrix} dx_i \tag{7}$$

where μ_0 is the free space magnetic permeability, x_i, y_i and z_i represent the points (i) in the conductor position. Equation (7) characterize MF in point (x_o, y_o, z_o) originated by (i) conductor. The field density can be approximated through of (9), (10) and (11).

$$\vec{B}_{xi} = \frac{\mu_0 I_i}{4\pi} \sum_{-\frac{L}{2}}^{\frac{L}{2}} \frac{\left(-\sinh(\alpha x_i)\,(y_0 - y_i)\right)}{|\vec{r}|^3} \tag{8}$$

$$\vec{B}_{yi} = \frac{\mu_0 I_i}{4\pi} \sum_{-\frac{L}{2}}^{\frac{L}{2}} \frac{[(x_0 - x_i)\sinh(\alpha x_i) - (z_0 - z_i)]}{|\vec{r}|^3} \tag{9}$$

Substituting z_i from (4) in (9) results in (10)

$$\vec{B}_{yi} = \frac{\mu_0 I_i}{4\pi} \sum_{-\frac{L}{2}}^{\frac{L}{2}} \frac{1}{|\vec{r}|^3} \left[(x_0 - x_i)\sinh(\alpha x_i) - \left(z_0 - \frac{1}{\alpha}(\cosh(\alpha x_i) - 1)\right)\right] \tag{10}$$

$$\vec{B}_{zi} = -\frac{\mu_0 I_i}{4\pi} \sum_{-\frac{L}{2}}^{\frac{L}{2}} \frac{(y_0 - y_i)}{|\vec{r}|^3} \tag{11}$$

Equation (8) is equal to zero, (10) represents how the conductor catenary has influence on MF and (11)

is distance MF interference. Magnetic flux density $\vec{B}_{yi}$ is the component that can be collected by the prototype and calculated by (10).

3. Approximated calculation of the magnetic flux density

An interesting simplified method for electric and magnetic field calculations was presented by Roscoe et al. [13]. It is based on the fact that the magnetic flux density B produced by the current circulating through a fraction of the conductor defined by dl can be calculated using the Biot-Savart's Law [14] showed in (1).

The Biot-Savart's Law in (1) can be transformed into the expression shown in (12), and it can be applied to calculate the magnetic field produced by an overhead power transmission with a current i_i.

$$dB = \frac{\mu_0 i_i}{4\pi b}(\cos\alpha_1 - cos\alpha_2)\left(\frac{d\boldsymbol{l}}{l} \times \frac{\boldsymbol{b}}{b}\right) \quad (12)$$

where $\boldsymbol{b}$ is an orthogonal distance to $d\boldsymbol{l}$, to a generic observation point from $d\boldsymbol{l}$. The line length is defined by l. Angles α_1 and α_2 are defined between the beginning and the end of conductor $d\boldsymbol{l}$, as the reference observation point, as can be seen in Figure 2.

The start point ("c") of the $d\boldsymbol{l}$ conductor is represented by P(x_c, y_c, z_c), while the end point is identified by P(x_f, y_f, z_f) on the 3 axes. The observation point of the magnetic field is arbitrary, being identified by P(x_o, y_o, z_o).

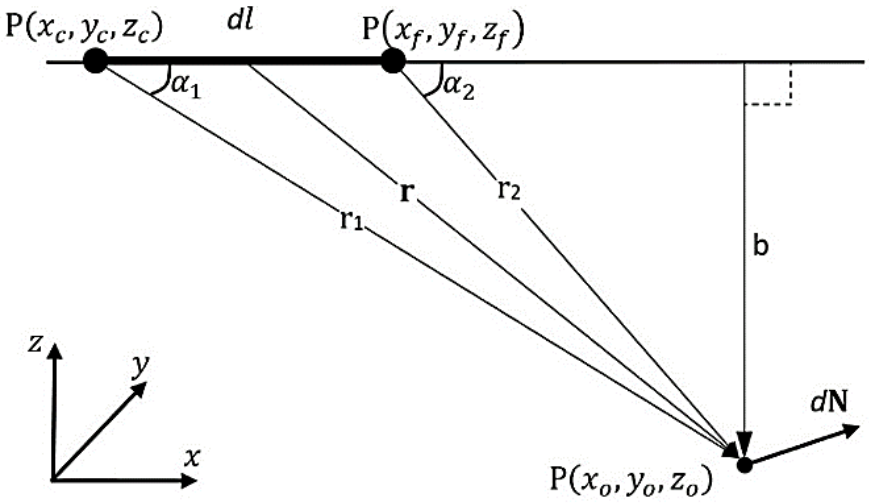

Figure 2. Magnetic field density characterization by simplified way.

The calculation was performed considering $d\boldsymbol{l}$, therefore the magnetic flux density obtained will be dB. Magnetic flux density that is obtained by (1), generates three components defined by $\overrightarrow{dB_x}$, $\overrightarrow{dB_y}$ and $\overrightarrow{dB_z}$ in three orthogonal axes as in (13).

$$dB = (dB_x, dB_y, dB_z) \quad (13)$$

This expression is valid for a single conductor, but if there were several parallel conductors, the individual components must be summed in the *x, y,* and *z* directions, as shown in (14). The final equation will give the three components B_{sx}, B_{sy} as B_{sz} valid for the same instant of time, defined by *t*.

$$B(t) = \left(B_{sx}(t), B_{sy}(t), B_{sz}(t)\right) \quad (14)$$

Then *B(t)* can be calculated as (15).

$$B(t) = \left(\sum dB_x(t), \sum dB_y(t), \sum dB_z(t)\right) \quad (15)$$

The magnetic flux density vector modulus *B* at time *t* can be determined by (16).

$$|B(t)| = \sqrt{B_{sx}(t)^2 + B_{sy}(t)^2 + B_{sz}(t)^2} \quad (16)$$

Considering that the overhead power transmission line is a balanced three-phase system, and that the angles between current phases are 120° (2π/3), currents i_1, i_2, and i_3 will have amplitude I_m and a ω angular frequency ($2\pi f$).

$$i_i = I_m \cos\left(\omega t - \frac{(i-1)2\pi}{3}\right) \rightarrow i = \{1,2,3\} \quad (17)$$

The root mean square of magnetic flux density can be obtained from (18).

$$B_{rms}(t) = \sqrt{\int_{t-T}^{t} \frac{1}{T} B^2(\tau)} \quad (18)$$

The magnetic flux density magnitude *B* is defined by (18), $T = 0{,}01666\ s$ is the period, and τ is an auxiliary integration variable. These expressions were codified in Matlab, based on a simple tower structure to calculate the magnetic flux density modules, as it is presented in the following section.

4. Prototype Implementation

The parts of the prototype built for the experiments are shown in Figure 3, formed by 4 cylindrical iron rods of a 1 m length. Each bar has a diameter of 19 mm, coiled with 2450 turns of copper each.

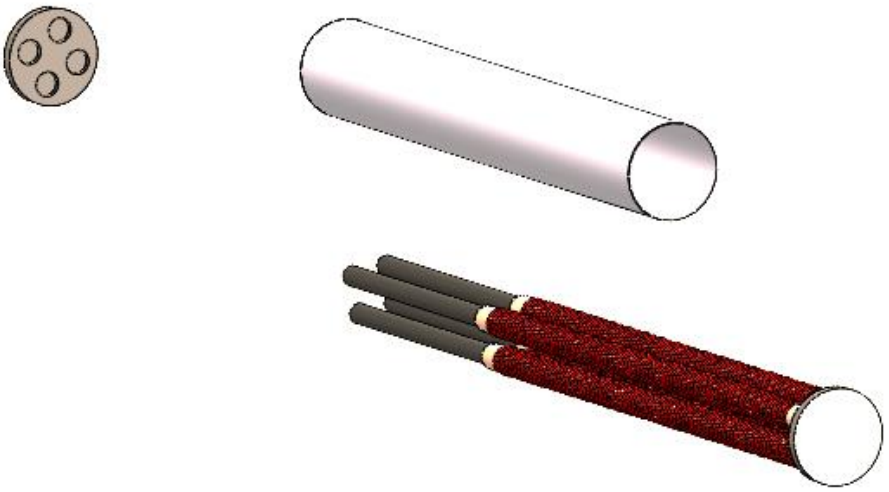

Figure 3. Internal structure of the prototype with exploded view showing the 4 iron bar rods with the copper turns.

Each solenoid was wound with a single layer. The copper wire has a diameter of approximately 0.4 mm and was wound onto a 1 mm thick PVC pipe, avoiding contact with the iron rod. The four bars are supported by two 1.8 cm Nylon 6.0, on which are resting the iron rods, fixing them inside the PVC tube of 7.2 cm in diameter. The outside of the tube has been covered with a ground aluminum foil film which was grounded during the measurement process. The only face of the unshielded aluminum tube was the face pointing the TL. The solenoid wire connections are in parallel and one of the covers was placed on the output terminal of the arrangement

The magnetic flux density can be obtained in the mounted structure by the Faraday's Law, by the expression of the open-circuit voltage V_{oc}, as can be seen in (19).

$$V_{OC} = 2\pi f \mu_{ef} N(\pi r^2) B \tag{19}$$

where B is magnetic flux density component in parallel to the axis of the arrangement, f is the operating frequency and r is the rod radius [15].

The core effective permeability μ_{ef} of the built solenoid can be replaced by the relative permeability of the material used in the core μ_r. Because there is not significant spacing between the solenoid and core winding, in (20) the solenoid inductance is calculated by

$$L_a = \frac{[\mu_0 \mu_r (\pi r^2) N^2]}{[l + 0{,}9(r)]} \tag{20}$$

To transfer maximum power, it was used a low input impedance stage with the required impedance coupling. Considering that the load is resistive, the inductance L_a should be compensated by a capacitance, as determined by (21) at an operating frequency f.

$$C_s = \frac{1}{[(2\pi f)^2 L_a]} \tag{21}$$

Thus, load R_L must be equal to R_a, which is calculated by (24). Since the inductor generates an open circuit voltage V_{OC} under a magnetic field B, the output voltage V_{out} will be half the open circuit voltage given by (22).

$$V_{out} = \frac{1}{2} V_{OC} = \pi f \mu_r N(\pi r^2) B \tag{22}$$

The equivalent circuit is shown in Figure 4 as modified from the one presented in IEEE Std 1308 (1995b), without the parasitic capacitance, due to the low frequency of the existing signal (50 or 60 Hz).

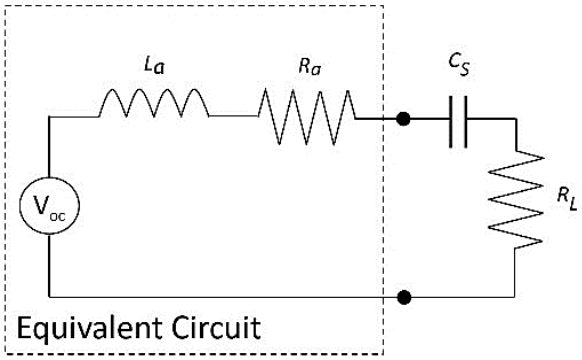

Figure 4. Open circuit equivalent model between dotted antenna lines.

The output power per unit volume can be determined by using the core length of the following relationship:

$$\frac{P_{saída}}{V_{ol}} = \frac{\left(\frac{V_{OC}}{2}\right)^2}{\frac{R_a}{[\pi r^2 h]}} = \frac{\left[\frac{(\pi f \mu_r N(\pi r^2) B)^2}{R_a}\right]}{[\pi r^2 h]} \tag{23}$$

where h is the solenoid height, ρ is resistance per length unit of the used cooper wire.

Under the parameters of Table 2 for R_a, L_a and C_s used to compensate the equivalent inductance. The value R_a is obtained from (24).

$$R_a = \rho N(2\pi r) \tag{24}$$

Table 2. Parameters of the equivalent circuit.

$R_a\ (\Omega)$	$L_a\ (H)$	$C_s\ (\mu F)$
23.8	0.385	73,6

Replacing (24) in (23) and simplifying, results in (25).

$$\frac{P_{saída}}{V_{ol}} = \frac{2\pi^2 r N \mu_r^2 f^2 B^2}{4\rho l} \tag{25}$$

The expressions obtained in this section allow to configure the acquisition circuit, and to continue with the processing signal using the embedded circuit. Relation (25) allows an interesting notion of the output dependence on the solenoid geometric proportions.

5. Magnetic field measurements

In order to carry out the measurements of the EM fields of a distribution line of 13.8 kV with a gap between towers of 40 m, with a cable line with Sparrow type steel core, with a 100 A-circulating current. Magnetic field levels were referenced to middle point of the imaginary parallel line to the axis joining the two towers, following a perpendicular line to the two towers. Figure 5 shows the positioning pattern of the experimental prototype. Five field readings were performed on the 3 axes with a ICEL commercial meter model EM-8000 Series No. E8000.0121 (ICEL, 2008) and a Minipa digital oscilloscope, model MO 2250 DC.

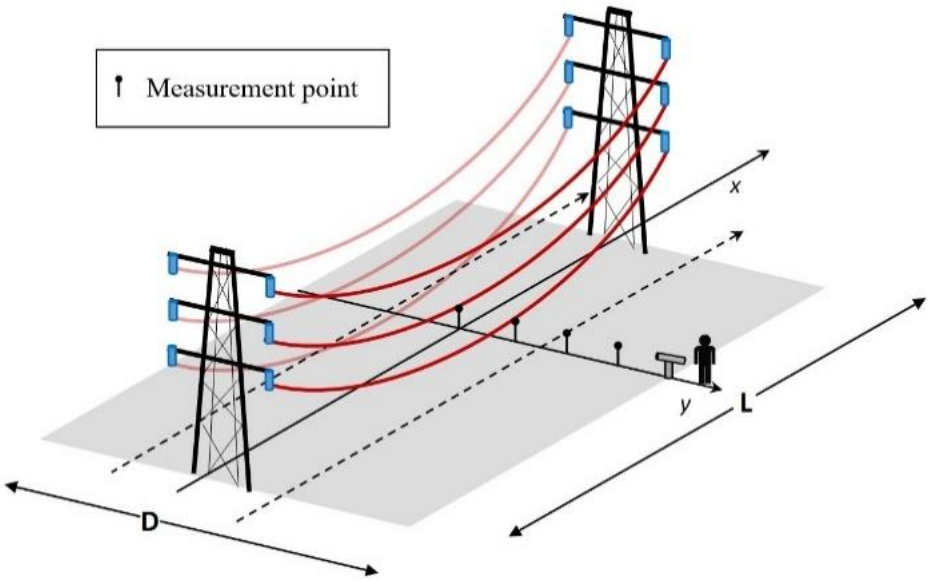

Figure 5. Points for monitoring a transmission line.

Figure 6 shows the positioned prototype placed at a height of 1 m from the ground level, supported by a wooden tripod in order to minimize interferences on the measurements, following the IEEE Std 644 644 (IEEE, 1995). The prototype was positioned 1 m above the ground level on wood tripod in order to minimize any interference on the measurements. Readings started from a distance of 30 m and going ahead by 5 m steps until reaching the axes center, as seen in Figure 5.

Figure 6. Prototype placed in front of 13.8 kV distribution line.

The experimental distribution line used along the tests passes through the campus of the Federal University of Rondônia (Brazil) being one of the reasons for selecting it. This location offered sheltering from atmospheric discharges, protection against rainfall and it is away from any interference generated by any environmental conditioning equipment. The environmental conditions during the reading tests were: temperature at 35 ºC and relative humidity of 86%.

The magnetic flux density generated by the line induced voltage on the prototype is detailed in (19). The voltage values obtained with this equation allow a comparison between the readings performed with the implemented prototype and the ones from the theoretical predictions under operating conditions shown in Table 4 of section VI.

Figure 7 shows the complete system to monitor the magnetic fields presented in this npaper. The basic circuit is emphasized with dotted lines, considering that induced voltage values are low in amplitude (nearly microvolts), the signal was then amplified and conditioned to be processed later by an embedded circuit able to process data to determine the value of B through (19).

Signal conditioning has been performed by the circuit shown in Figure 8. The circuit is composed of three stages. The first stage was implemented by the Texas Instrument amplifier INA122 with a CMRR = 90 dB; the second stage is an active fourth-pass bandpass filter with the center frequency at 60 Hz and a bandwidth of 40 Hz. The last stage was used to adjust the gain with an TL072 amplifier. Total circuit absolute gain owas equal to 500 or 54 dB with respect to the field level found at monitoring point.

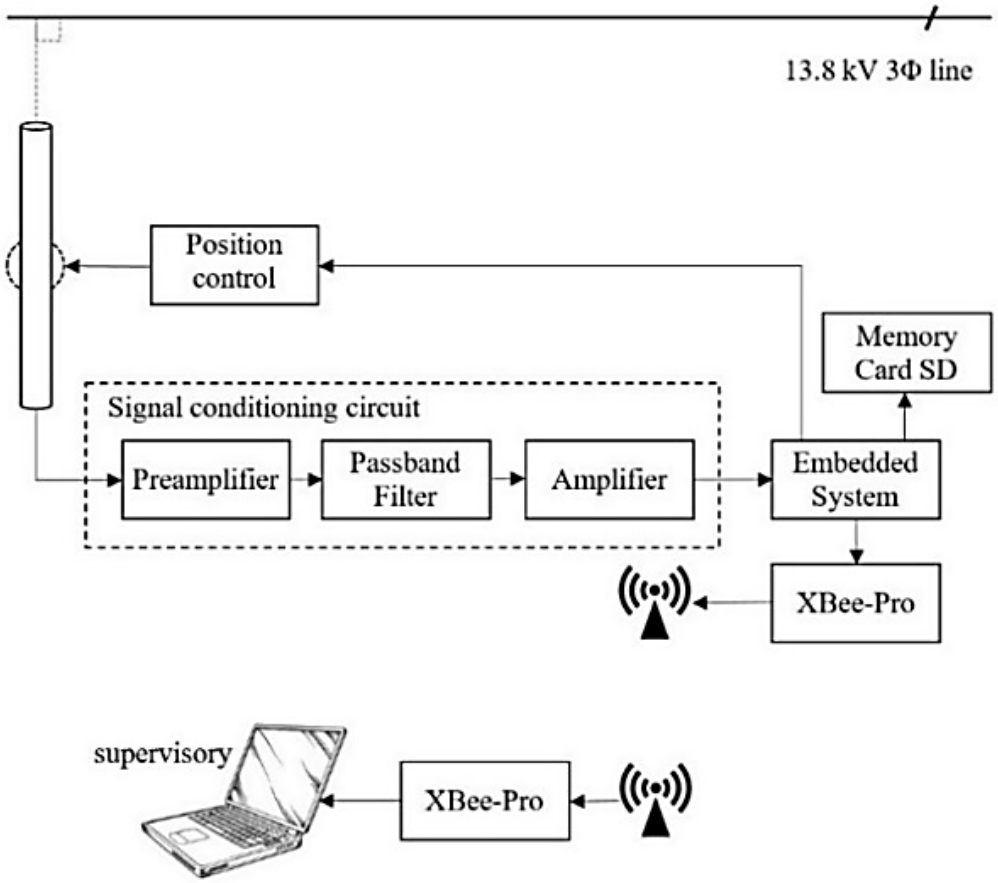

Figure 7. Data acquisition circuit to perform the prototype readings.

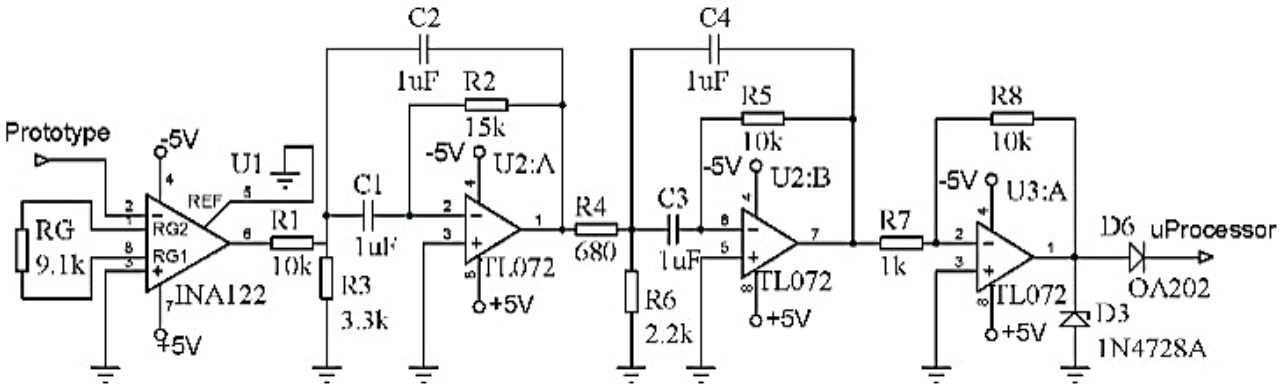

Figure 8. Signal Conditioning Circuit.

Table 3 displays the level ratios and gains obtained by the signal conditioner circuit in order to avoid any signal distortions.

Table 3. Absolute circuit gains for different density levels of the measured magnetic flux.

B [T]	V_{oc} [V]	Gain	V_{in}Embbed [V]
6.10^{-8}	$3.14.10^{-3}$	500	1.57
6.10^{-7}	$3.14.10^{-2}$	100	3.14

6.10^{-6}	$3.14.10^{-1}$	10	3.14
6.10^{-5}	3.14	1	3.14
6.10^{-4}	31.4	0.1	3.14
1.10^{-3}	52.4	0.01	0.524

For levels above 6 μT, the circuit of Figure 8 required modifications, such as suppression of the last amplifier and a voltage divider arrangement for a magnetic flux density of 1000 μT. The measured levels were compared to the calculated theoretical values as listed in Figure 9.

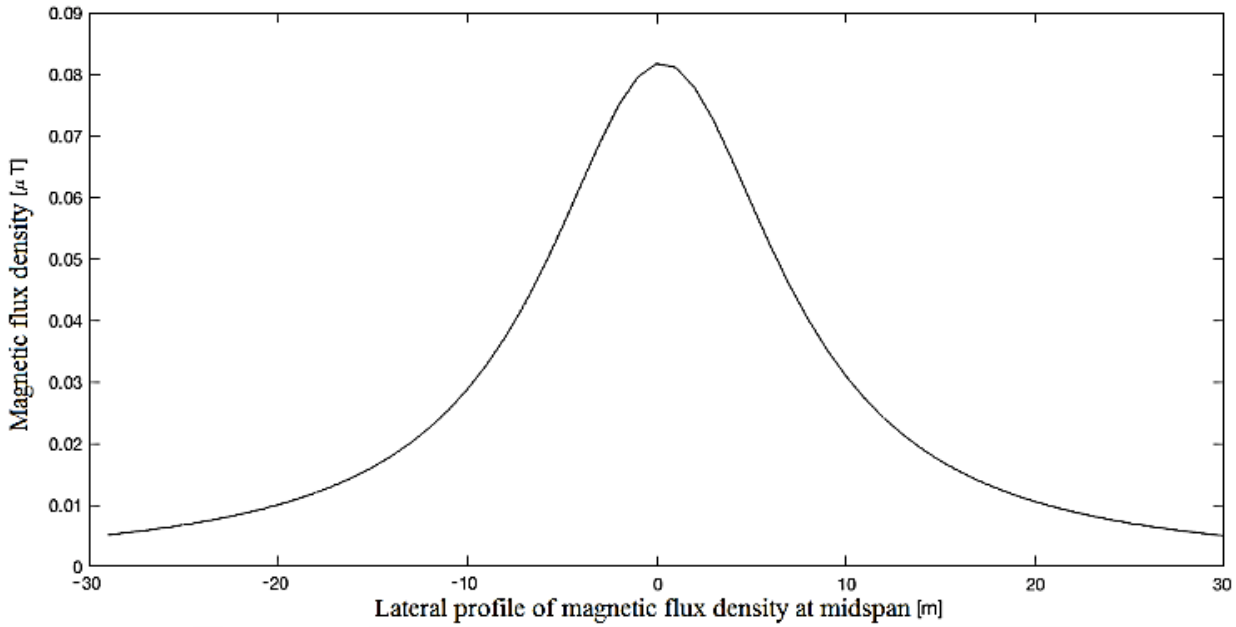

Figure 9. Magnetic Field levels for 13.8 kV distribution line.

Although the arrangement used during the EM measurements were not exactly an antenna, the prototype directivity was simulated through a computational simulation. The software chosen was the Ansoft's HFSS, ver 15.0. Thus, using a computer compatible with 8 cores, 28 Gb of RAM with the Windows operating system, version 10, and 15 Gb of disk free space to store the results obtained by the program, the graph of the directivity was plotted as in Figure 10.

With a driven voltage of 1 V and 60 Hz center frequency, according to the reciprocity law, the radiation pattern of a transmitting antenna looks like the receiving antenna diagram. The simulation started with 10 turns and increased during simulations up to 250 turns. After this number of turns the computational resources were not practical to finalize a more detailed simulation with success.

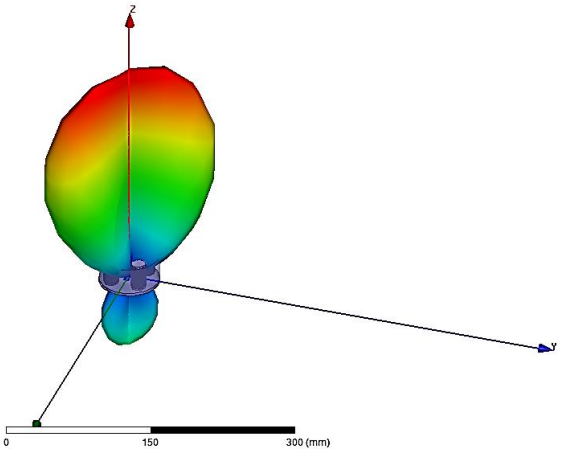

Figure 10. Directivity radiation diagram of the field generated by the assembled arrangement.

6. Results and discussion

Table 5 lists the magnetic flux density results obtained for distances between 0 and 30 m. In the second column of this table, is displayed the reference theoretical calculation considering the cable electrical physical parameters. In the third and fourth columns are shown the measurements obtained with the prototype and manual meter, respectively. The last column lists an approximation reached applying a 6-th order regression polynomial. The ratio in (26) defines the used polynomial expression.

$$ratio = \sum_{n=0}^{6} a_n \, d^n \tag{26}$$

where *d* is monitoring distance.

The ratio let to fit prototype values to theoretical levels at distances between 0 to 30 m as predicted by (26), with the residual sum of squares $rss = 5.451869222 \cdot 10^{-16}$, R_2=1 and the coefficients shown in Table 4.

Table 4. Coefficients values of 6th order regression polynomial.

Coefficient	Value
a_6	$1.555758547 \cdot 10^{-7}$
a_5	$-1.226720263 \cdot 10^{-5}$
a_4	$3.76711781 \cdot 10^{-4}$
a_3	$-5.802067755 \cdot 10^{-3}$
a_2	$4.92151768 \cdot 10^{-2}$
a_1	$-1.994529988 \cdot 10^{-1}$
a_0	0 .4325016518

They were calculated several lower approximations, nonetheless the 6-th order was the one which had a better approximation.

In Figure 10 is plotted the three first values of the magnetic flux density as compiled in Table 5. It can be seen that theoretical magnetic flux density had less variation than those values obtained by the prototype and meter used. The meter obtained a higher value because the z-component was more significant when positioned below the distribution line while the prototype had a lower level because of its proximity to the line. However, this difference in the first 15 m decreased with an exponential trend between 20 and 30 m, which is the proposed distance by this research.

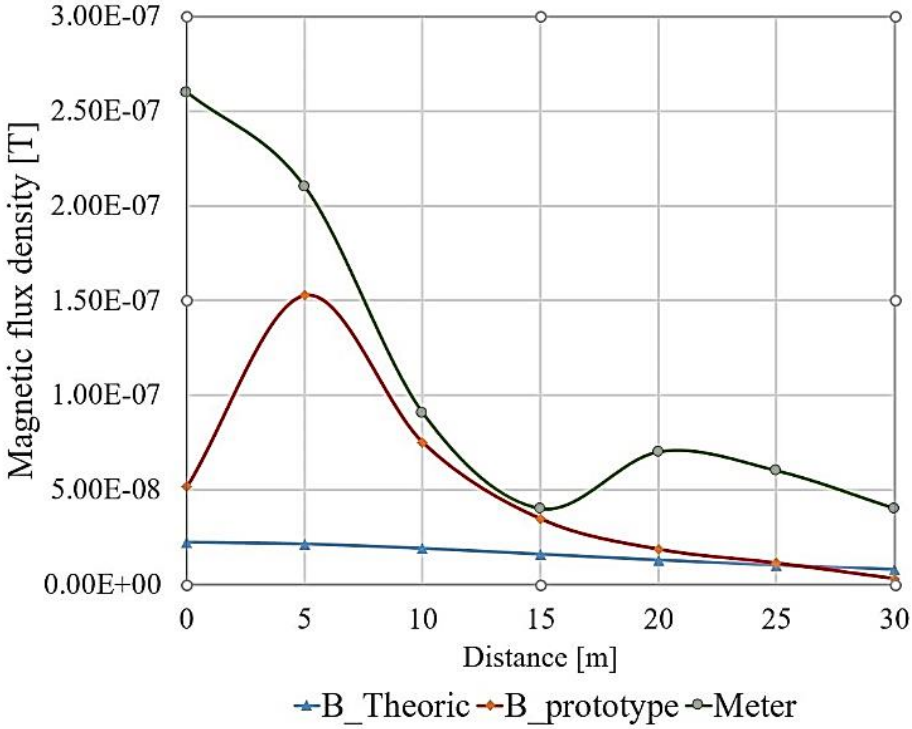

Figure 11. Magnetic flux density plotted by theoretical calculation, prototype values and meter readings.

In Figure 12 is plotted the values of the theoretical and the polynomial approximations. The time was selected as reference for the theoretical comparative values because the input parameters were already known, as the line current, distance between towers and conductor type.

Table 5. Magnetic flux density levels obtained for a distribution line with current 100 A for distances between 0 to 30 m.

Dist. [m]	Theoretical [T]	Prototype [T]	Meter [T]	Approx. by a 6-th order poly [T]
0	$2.227\ 10^{-8}$	$5.15\ 10^{-8}$	$2.60\ 10^{-8}$	$2.227\ 10^{-8}$
5	$2.137\ 10^{-8}$	$1.53\ 10^{-7}$	$2.10\ 10^{-7}$	$2.137\ 10^{-8}$
10	$1.901\ 10^{-8}$	$7.5\ 10^{-8}$	$9.05\ 10^{-8}$	$1.901\ 10^{-8}$
15	$1.593\ 10^{-8}$	$3.46\ 10^{-8}$	$4.00\ 10^{-8}$	$1.593\ 10^{-8}$
20	$1.282\ 10^{-8}$	$1.86\ 10^{-8}$	$7.00\ 10^{-8}$	$1.282\ 10^{-8}$
25	$1.009\ 10^{-8}$	$1.14\ 10^{-8}$	$6{,}00\ 10^{-8}$	$1{,}009\ 10^{-8}$
30	$7.869\ 10^{-8}$	$3.09\ 10^{-9}$	$4.00\ 10^{-8}$	$7.869\ 10^{-9}$

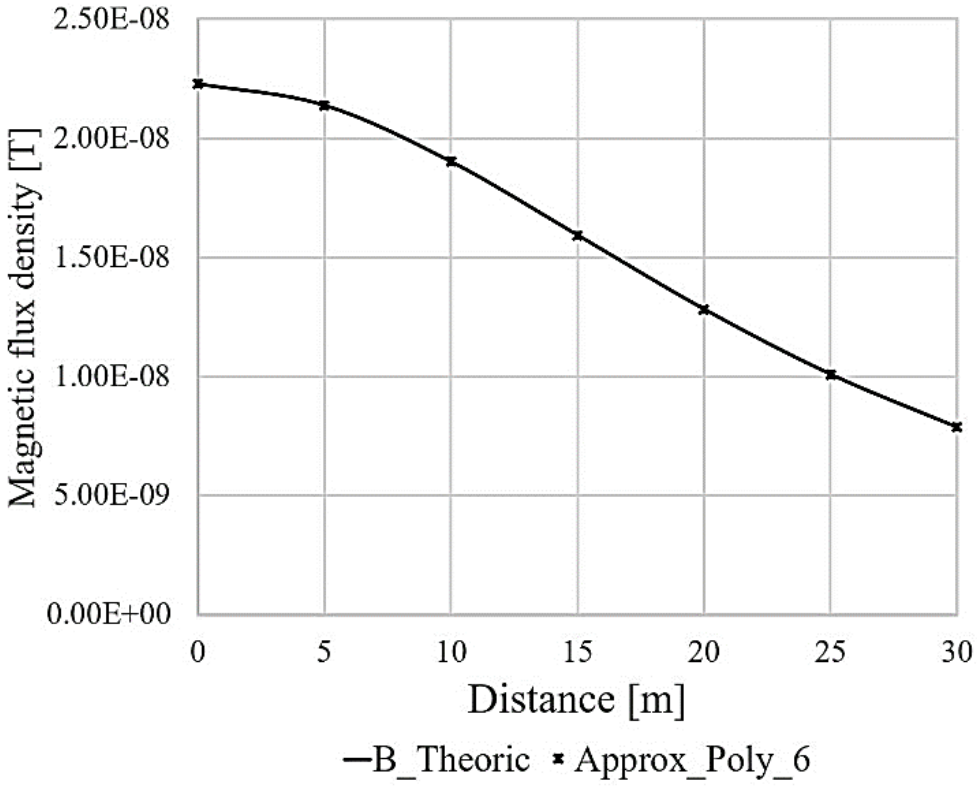

Figure 12. Theoretical magnetic flux density and values calculated by 6-th order polynomial approximation factor applied in prototype.

7. Conclusion

This paper proposes an implementation of a remote monitoring prototype of magnetic flux density with the use of materials easily found in local market. The prototype dimensions as presented here can be reduced with the use of core materials with higher magnetic permeability as observed in the equations as presented in Section 4.

The theoretical values of the magnetic flux density for distances greater than 20 m from the imaginary axis are very close to the values measured by the prototype.

The choice of a single axis structure to capture the magnetic field is based on the safety of the physical dimensions according the orders of magnitude of the signal to be monitored. It was observed that the selected local where the tests were performed presented a high index (9) of atmospheric discharges [16].

The approximate values obtained through theoretical equations provide an interesting estimative for the actual existing magnetic field density. Taking into account that the field density depends on the nominal current and on a few physical characteristics of the cables, it is concluded that there is a limited spacing for arrangement of the conductors and the height to support the 3-phase circuit.

The accuracy of the existing magnetic field calculations can be improved by using information from the substation's current transformer, which will allow to have better evaluation of the magnetic field produced by a real time current circulation through the TL.

8. Acknowledgement

The authors are very grateful to CAPES and CEESP/UFSM for the support provided to make this work possible.

9. References

[1] R. Kavet, M. A. Stuchly, W. H. Bailey, and T. D. Bracken, "Evaluation of biological effects, dosimetric models, and exposure assessment related to ELF electric- and magnetic-field guidelines," Appl Occup Env. Hyg, vol. 16, no. 12, pp. 1118–1138, 2001.

[2] H. Jia, "The influence of extremely low-frequency magnetic field and magnetic nanoparticle on A β40 aggregation in Vitro," IEEE Trans. Electromagn., vol. 51, no. 11, p. 2015, 2015.

[3] Y. Cui, X. Liu, T. Yang, Y.-A. Mei, and C. Hu, "Exposure to extremely low-frequency electromagnetic fields inhibits T-type calcium channels via AA/LTE4 signaling pathway.," Cell Calcium, vol. 55, no. 1, pp. 48–58, 2014.

[4] A. Komaki, A. Khalili, I. Salehi, S. Shahidi, and A. Sarihi, "Effects of exposure to an extremely low frequency electromagnetic field on hippocampal long-term potentiation in rat," Brain Res., vol. 1564, pp. 1–8, 2014.

[5] T. Barsam, M. R. Monazzam, A. A. Haghdoost, M. R. Ghotbi, and S. F. Dehghan, "Effect of extremely low frequency electromagnetic field exposure on sleep quality in high voltage substations.," Iranian J. Environ. Health Sci. Eng., vol. 9, no. 1, p. 15, 2012.

[6] IARC, Working Group on the Evaluation of Carcinogenic Risks to Humans and World Health Organization and International Agency for Research on Cancer. Non-ionizing Radiation: Static and extremely low-frequency (ELF) electric and magnetic fields, vol. 80. Lyon, France: World Health Organization, 2002.

[7] N. McNelis, "EU communications on the precautionary principle," J. Int. Econ. Law, vol. 3, no. February 1998, pp. 545–551, 2000.

[8] ICNIRP, "ICNIRP statement on the 'guidelines for limiting exposure to time-varying electric, magnetic, and electromagnetic fields (up to 300 ghz),'" Health Phys., vol. 74, no. 4, pp. 494–522, 1998.

[9] ICNIRP, "Guidelines for Limiting Exposure to Time-Varying Electric and Magnetic Fields (1Hz to 100 KHz)," Health Phys., vol. 99, no. 1, p. 112, 2010.

[10] J. Swanson, "Power-frequency EMF Exposure Standards applicable in Europe and elsewhere," 2014. [Online]. Available: http://www.emfs.info/wp-content/uploads/2014/07/standards-table-revision-5l-July-2014.pdf.

[11] J. Liu, W. Ruan, S. Fortin, and F. P. Dawalibi, "Electromagnetic fields near high voltage electrical power lines: a parametric analysis," in Power System Technology, 2002. Proceedings. PowerCon 2002. International Conference on, 2002, vol. 1, pp. 401–408.

[12] A. H. Khawaja and Q. Huang, "Characteristic estimation of high voltage transmission line conductors with simultaneous magnetic field and current measurements," 2016 IEEE International Instrumentation and Measurement Technology Conference Proceedings. pp. 1–6, 2016.

[13] M. D. J. Roscoe, N. M. and and L. Fraser, "A Novel Inductive Electromagnetic Energy Harvester For Condition Monitoring Sensors," in Proceedings of the 2010 International Conference on Condition Monitoring and Diagnosis -CMD 2010, Tokyo, Japan, September 6 - 11, 2010, pp. 615–618.

[14] X. Sun, Q. Huang, L. J. Jiang, and P. W. T. Pong, "Overhead high-voltage transmission-line current monitoring by magnetoresistive sensors and current source reconstruction at transmission tower," IEEE Trans. Magn., vol. 50, no. 1, 2014.

[15] N. M. Roscoe and M. D. Judd, "Harvesting Energy From Magnetic Fields to Power Condition Monitoring Sensors," IEEE Sens. J., vol. 13, no. 6, pp. 2263–2270, 2013.

[16] ONS, "Operador Nacional do Sistema. Mapas de Densidade de Descargas Atmosféricas," 30 de setembro 2015, 2015. [Online]. Available: http://www.ons.org.br/conheca_sistema /mapas_sin.aspx. [Accessed: 15-Nov-2016].